Title

External oxidant-free remediation of antibiotics: Activation of oxygen molecules to generate hydroxyl radicals using Co-Fe3S4 nanoflowers

Authors

Xu, Jingyi
Tan, Xianjun
Ding, Wenhui
et al.

Publication Date

2023-05-01

DOI

10.1016/j.cej.2023.142465

Chemical Engineering Journal 463 (2023) 142465

Contents lists available at ScienceDirect

Chemical Engineering Journal

journal homepage: www.elsevier.com/locate/cej

External oxidant-free remediation of antibiotics: Activation of oxygen molecules to generate hydroxyl radicals using Co-Fe_3S_4 nanoflowers

Jingyi Xu [a], Xianjun Tan [a], Wenhui Ding [a], Arturo A. Keller [b], Yuxiong Huang [a,*]

[a] Tsinghua-Berkeley Shenzhen Institute (TBSI), Shenzhen International Graduate School (SIGS), Tsinghua University, Shenzhen 518055, PR China
[b] Bren School of Environmental Science and Management, University of California, Santa Barbara, CA 93106, United States

ARTICLE INFO

Keywords:
O_2 activation
Dissociative adsorption
Antibiotic
Oxidant free
Greigite
Degradation

ABSTRACT

To overcome the obstacles of adding oxidants for the decontamination of antibiotics in natural aqueous environment, an external oxidant-free system was developed to *in-situ* generate reactive oxygen species (ROS) through the activation of dissolved oxygen molecules (O_2). Guided by density functional theory (DFT) calculation, cobalt-doped Fe_3S_4 (Co-Fe_3S_4) nanoflowers were designed and synthesized, which exhibited superior O_2 adsorption and activation ability. Co-Fe_3S_4 triggered a long-lasting generation of •OH with a high yield of 16.63 μM •OH, which was 3 times higher than that of Fe_3S_4. Furthermore, use of Co-Fe_3S_4 resulted in a 7.33-fold improvement in sulfamethoxazole's degradation rate and boosted the degradation efficiency from 43% to over 90% in the long-run experiments compared to Fe_3S_4. With $^{18}O_2$ isotopic investigations, we quantitatively revealed that •OH was generated via O_2′s one-step dissociative adsorption process and the directional electron transfer contributed by structural S(-II). Without the addition of external oxidants (e.g., H_2O_2, O_3), we have reported an efficient one-step activation of O_2 to generate ROS for effective degradation of antibiotics. Hence, we have provided a new strategy for the control of emerging organics in natural water systems, as well as shed light on the mechanisms of *in-situ* •OH generation.

1. Introduction

The continuous release of antibiotics during their life cycle of manufacturing, application, excretions, and disposal, has led to a substantial accumulation of antibiotics in natural water bodies (e.g., groundwater[1–3], rivers[4,5], lakes[6], etc.). The occurrence of antibiotics poses significant threats to ecosystems and public health by the induction and dissemination of antibiotic resistance bacteria.[7] Hence, it is urgent to provide effective in-situ remediation techniques for the control of antibiotics in natural water bodies. As one of the most promising techniques, advanced oxidation processes have been extensively applied for the remediation of various contaminants (e.g., antibiotics[8–11], phenol[12,13], pesticides[14,15], etc.). Typically, external addition of oxidants (e.g., H_2O_2[16–18], ozone[19,20], persulfate[21–23]) is required to generate reactive oxygen species (ROS) to degrade pollutants. Unlike the engineered systems (e.g., wastewater treatment plant), the external addition of oxidants to natural water bodies would consume a relatively large amount of chemicals[24], which may further pose ecotoxicological risks such as the formation of disinfection byproducts[25,26].

Recently, more and more attention has been redirected to utilizing dissolved O_2 in water for antibiotics remediation[27–29]. However, it's challenging to directly convert O_2 into ROS due to the thermodynamic stability of O_2 in its triplet ground state[30]. The involvement of heterogeneous catalysts would contribute to the O_2 activation through electron transferring to the π* orbital of O_2.[31,32] Iron-sulfur minerals are generally considered as preferred catalysts to promote ROS generation due to their transition chemical states and rich active sites on the surface[33]. Dong et al.[27,29] reported the spontaneous •OH generation from the oxidation of mackinawite (FeS), which was applied for the remediation of arsenic and phenol. Being the naturally abundant ferromagnetic iron-sulfur mineral, greigite (Fe_3S_4) has been widely applied in heterogeneous AOPs. Liu et al.[34,35] found an extensive peroxidase-like activity of Fe_3S_4, and applied Fe_3S_4 to remove arsenic. Moreover, Shi et al.[36] reported Fe_3S_4/H_2O_2 system to degrade atrazine using $\bullet O_2^-$ produced from O_2 under light irritation, demonstrating Fe_3S_4′s potential to activate O_2 for degrading organic pollutants.

On the other hand, the poor adsorption of dissolved O_2 onto the surface of the catalysts remains a major challenge for using O_2 to degrade contaminants[35,37]. Montemore et al.[38] proposed a

* Corresponding author.
E-mail address: huang_yuxiong@sz.tsinghua.edu.cn (Y. Huang).

https://doi.org/10.1016/j.cej.2023.142465
Received 12 January 2023; Received in revised form 2 March 2023; Accepted 14 March 2023
Available online 17 March 2023

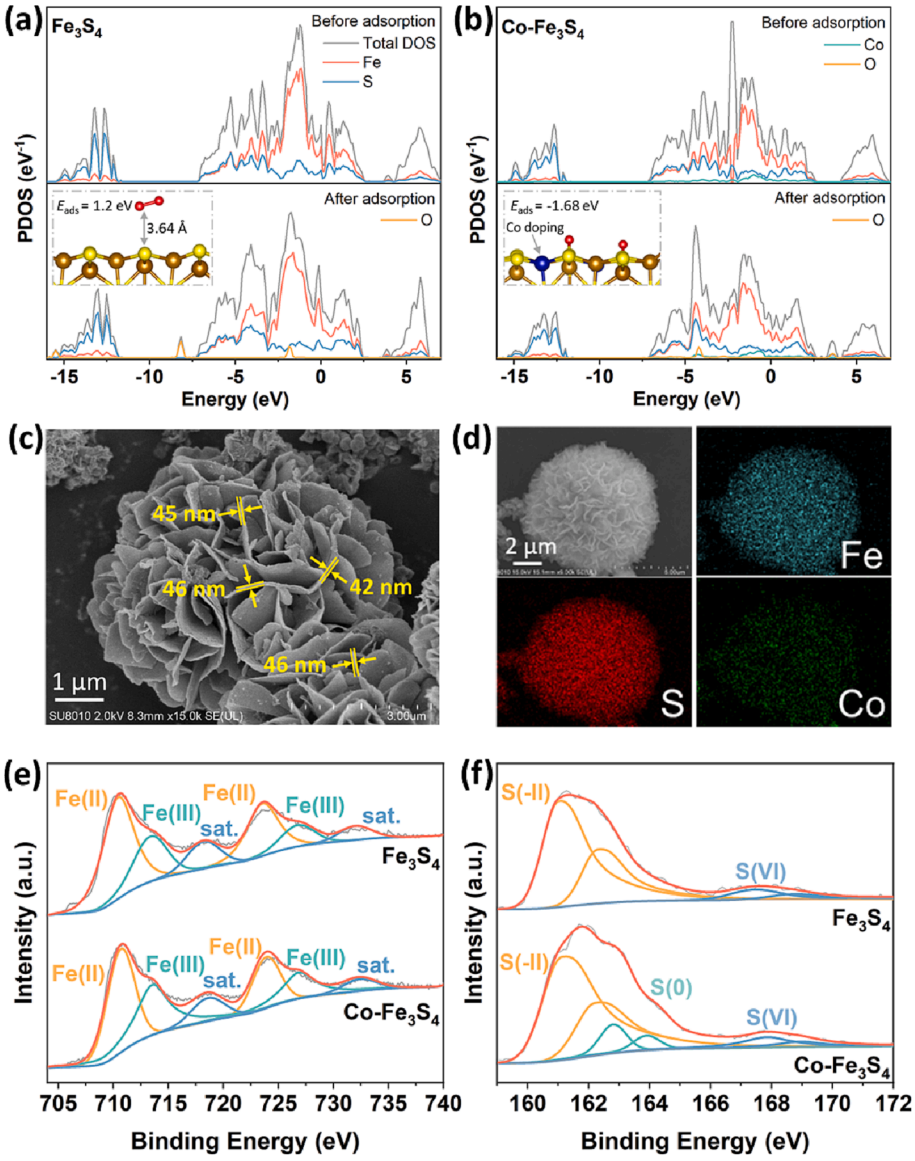

Fig. 1. DOS of (a) Fe_3S_4 and (b) Co-Fe_3S_4 nanoflowers before and after O_2 adsorption, respectively. The insets show the corresponding relaxed adsorption structures of oxygen molecules adsorbed on the surface of Fe_3S_4 and Co-Fe_3S_4. Color scheme: Fe = brown, S = yellow, O = red, and Co = blue. (c) SEM images of the nanoflowers, and (d) elemental mapping of Co-Fe_3S_4. XPS spectra of (e) Fe and (f) S in Fe_3S_4 and Co-Fe_3S_4.

periodic trend in the of metal surfaces to O_2 activation that metals with a mostly empty d shell, such as Co, Fe, and Rh, presented extremely low adsorption and dissociation barriers. Hence, modification of under-coordinated defect sites through doping with active transition metals has been considered as a promising method to improve the O_2 adsorption capacity and the catalytic performance[39–42]. Liu et al.[43] found a superior photocatalytic reactivity for CuS_4-modified $ZnInS_4$ nanosheets due to the better O_2 adsorption ability and more favorable electron transferring. Similarly, Zhao et al.[44] reported that Co-doped monolayer MoS_2 exhibits excellent O_2 adsorption capacity, which could generate activated oxygen atoms through a dissociation reaction. Thus, doping with transition metals (e.g., Co) in Fe_3S_4 may significantly improve the adsorption and activation ability of dissolved O_2, which have not been thoroughly investigated.

In this study, enhanced O_2 adsorption by doping Fe_3S_4 with Co was predicted via theoretical calculation. Guided by theoretical calculation, a Co-Fe_3S_4 catalyst was synthesized and evaluated for antibiotic degradation via the activation of dissolved O_2. The underlying mechanisms of O_2 conversion were revealed by conducting ^{18}O isotopic labeling remediations. Furthermore, the O_2 activation performance by Co-Fe_3S_4 was evaluated under various environmental conditions. We provide new insights on the Co-Fe_3S_4 assisted activation of O_2 into ROS to effectively degrade organic pollutants, which is a novel external-oxidant free *in-situ* chemical oxidation approach for the control of emerging organic pollutants.

2. Materials and methods

2.1. Chemical and materials

Analytical grade iron (III) chloride hexahydrate ($FeCl_3{\cdot}6H_2O$), thiourea ($CS(NH_2)_2$), and ethylene glycol (EG) were purchased from Sinopharm Chemical Reagent Co., Ltd. (Shanghai, China). Cobalt chloride hexahydrate ($CoCl_2{\cdot}6H_2O$), 5,5-dimethyl-1-pyrrolidine-N-oxide (DMPO), 2,2,6,6-tetramethylpiperidine (TEMP), benzoic acid (BA), 4-hydroxyl benzoic acid (4-HBA), *tert*-butanol (TBA) were purchased from Aladdin (Shanghai, China). All the chemicals were used without further purification. Ultra-pure water (Millipore Super Q system) with a

resistivity of 18.2 MΩ cm was used in the experiments.

2.2. Synthesis of Co-Fe_3S_4

The Co-Fe_3S_4 nanoflowers were prepared by a modified hydrothermal method[45]. Specifically, $FeCl_3{\cdot}6H_2O$ (3.0 mmol), $CoCl_2{\cdot}6H_2O$ (0.6 mmol), and thiourea (6.0 mmol) were dissolved in 60 mL of EG to form a carmine solution under magnetic stirring. The solution was then transferred into a 100 mL Teflon-lined stainless-steel autoclave and heated at 180 °C for 12 h. After cooling to room temperature, the product was collected and washed with DI water and ethanol thrice, then dried in a vacuum oven at 40 °C for 8 h. The proportion of Co within Co-Fe_3S_4 from 10% to 50% was tuned for comparison by adjusting the dosage of $CoCl_2{\cdot}6H_2O$ (from 0.3 mmol to 1.5 mmol) during the hydrothermal process. As a control, Fe_3S_4 was prepared by a similar process without the addition of $CoCl_2{\cdot}6H_2O$ during the synthesis process.

2.3. Degradation of antibiotic

The antibiotic degradation performance of Co-Fe_3S_4 was verified by different pollutants including sulfamethoxazole (SMX), sulfadiazine (SDZ), carbamazepine (CBZ) and ofloxacin (OFX), and SMX was chosen as the typical pollutant in the following experiments. In degradation experiment, 25 mg of catalyst were dispersed into 50 mL of a 10 mg/L sulfamethoxazole (SMX) aqueous solution in a 100 mL round-bottom flask (25 ± 1℃), shaken at 200 rpm. Flasks were covered with aluminum foil to avoid potential photochemical reactions and open to the atmosphere. Samples were collected at specific intervals and immediately quenched with 0.2 mL methanol. The solution was then centrifugated and filtered using a 0.22 μm polyethersulfone (PES) membrane before high-pressure liquid chromatography (HPLC) analysis.

To account for the contribution of O_2 to the removal of SMX, degradation experiments were also performed under N_2 and O_2 atmosphere. To explore the effect of pH, the initial pH of the SMX/catalyst solution was adjusted by HCl or NaOH to 3, 5, 7, and 10, respectively. Then, the pH value was monitored throughout the degradation process. In addition, the influence of water matrix was also investigated, by carrying out the SMX degradation experiments with the addition of 1 mM and 10 mM NaCl, Na_2SO_4, and NH_4HCO_3, respectively, and 1 mg/L and 10 mg/L of natural organic matter (humic acid). All the other procedures were the same as described above. All degradation experiments were conducted in triplicate. Additional details of characterization techniques and analytical methods are given in supporting information (SI).

2.4. Theoretical calculation

Theoretical calculations were performed using density functional theory (DFT) as implemented in the Vienna *ab initio* simulation package (VASP) code. A 4 × 4 × 1 supercell of Fe_3S_4 (1 1 0) facet with a 15 Å vacuum layer was constructed to mimic the Fe_3S_4 nanosheets, and the k-points were 2 × 2 × 1 for structure optimizations. Co-Fe_3S_4 nanosheets were constructed by substituting 20% of 5-coordinated Fe atoms on the top-layer with Co atoms. The energy cutoff was set at 500 eV, and the topmost five layers of the slab were allowed to relax until the energy and residual forces were less than 10^{-5} eV and 10^{-2} eV/Å, respectively.[46] To evaluate oxygen adsorption and decomposition on the surface of Fe_3S_4 and Co-Fe_3S_4, an oxygen molecule was placed 3 Å above the 4-coordinated Fe atom on the top-layer of Fe_3S_4 and Co-Fe_3S_4 respectively, and relaxed until converged. The adsorption energies E_{ads} were defined as: $E_{ads} = E_{adsorbate+surface} - E_{surface} - E_{adsorbate}$, where $E_{adsorbate+surface}$ represents the total energy of the oxygen molecule and the surface of Fe_3S_4 or Co-Fe_3S_4 in the equilibrium state, $E_{surface}$ and $E_{adsorbate}$ represent the total energy of oxygen molecular and surface alone, respectively. In addition, Bader charge analysis and density of state (DOS) analysis were adopted to characterize the charge transfer between the oxygen molecule and the material's surface.

3. Results and discussion

3.1. Theoretical calculation-guided design of Co-Fe_3S_4

According to the DFT theoretical calculation, Fe_3S_4 was thermodynamically unfavorable for O_2 adsorption with a positive adsorption energy of + 0.12 eV. Based on the DOS analysis, the d-states of Fe and p-states of S in Fe_3S_4 remained unchanged before and after O_2 adsorption (Fig. 1a), suggesting weak interactions between Fe_3S_4 and O_2. Furthermore, the distances between the O_2 molecule and Fe_3S_4 were enlarged from 3.00 Å to 3.64 Å, while no significant differences were observed for O-O bond length before and after O_2 adsorption (d(O-O) = 1.20 Å[47]). Therefore, minimal O_2 would be adsorbed onto Fe_3S_4. After doping Co onto Fe_3S_4, O_2 would be spontaneously adsorbed onto the Co-Fe_3S_4 surface with a negative adsorption energy of −1.68 eV and subsequently dissociated into two highly active •O (Fig. 1b). In addition, strong hybridization between atomic O and Fe and S atoms occurred after O_2 was adsorbed onto the Co-Fe_3S_4 surface, as a distinct peak of Fe-3d and S-2p formed at −4.2 eV and slightly diminished around the Fermi level. Consistent with Bader charge analysis, a charge of 1.69 e^- was transferred from the interacting Fe and S ions to the adsorbed O π_g orbital, which generated a significant electron-rich environment on the dissociative O atoms (Fig. S1). Thus, doping Co in Fe_3S_4 could not only enhance O_2 adsorption and dissociation but also facilitate the proton transfer to adsorbed O for higher reactivity.

Guided by the theoretical calculation, Co-Fe_3S_4 was prepared by doping Co in Fe_3S_4. Co-Fe_3S_4 nanosheets with approximate 45 nm of thickness exhibited uniform flower-like aggregates (Fig. 1c), which was similar to the morphology of Fe_3S_4 (Fig. S2). Elemental mapping demonstrated that Co was evenly distributed on Co-Fe_3S_4 (Fig. 1d), and the proportion of S, Fe, and Co was approximately 4:3:0.6 (Fig. S3, Table.S1). The crystalline phase of Co-Fe_3S_4 was examined by XRD (Fig. S4), and the main diffraction peaks of Co-Fe_3S_4 were well ascribed to the facets of cubic phase Fe_3S_4 (JCPDS no. 16–713). In addition, lattice spacings of 0.175 nm and 0.297 nm were observed in the HRTEM (Fig. S5), which were well-matched with the (4 4 0) and (3 1 1) facets of Fe_3S_4, respectively.

The doping of Co induced a change in the coordinating environment of Fe atoms in Co-Fe_3S_4 due to the bonding hybridization of Fe atoms to the nearest-neighbor Co atom[48]. The weakened electrons screening effect contributed to the slight shift of Fe(II) and Fe(III) peaks to the higher binding energies, as the binding energies of Fe(II) shifted from 710.6 (Fe_3S_4) to 710.9 eV (Co-Fe_3S_4) and 723.8 (Fe_3S_4) to 724.1 eV (Co-Fe_3S_4), and the binding energies of Fe(III) shifted from 713.6 and 726.8 (Fe_3S_4) to 713.7 and 726.9 eV (Co-Fe_3S_4) (Fig. 1e). Correspondingly, the dominant chemical state of S in Fe_3S_4 and Co-Fe_3S_4 were S(-II) and S(VI), as characteristic peaks arising at 161.0 and 168.0 eV (Fig. 1f). Besides, two more peaks at 162.4 and 163.4 were identified in the S-2p spectra of Co-Fe_3S_4, which can be attributed to S(0).

3.2. •OH-mediated degradation of antibiotics

Co-Fe_3S_4 exhibited outstanding remediation performance to various antibiotics including SMX, SDZ, CBZ, OFX, with removal efficiencies up to 91% (Fig.S6). Due to the stability of the degradation process, SMX was chosen as the indicator in the following experiments to investigate the degradation performance of Co-Fe_3S_4. Furthermore, the optimized doping ratios of Co was analyzed by ranging the proportion from 10% to 50%, and Co-Fe_3S_4 with 20% Co doping was proved to exhibit the best degradation performance (Fig.S7). Propriate proportion of Co doping (less than30%) could promote the O_2 adsorption of Fe_3S_4 to improve degradation efficiency. Meanwhile, the increase of Co proportion would also result in the generation of CoS_x (Fig.S8), which would compete of

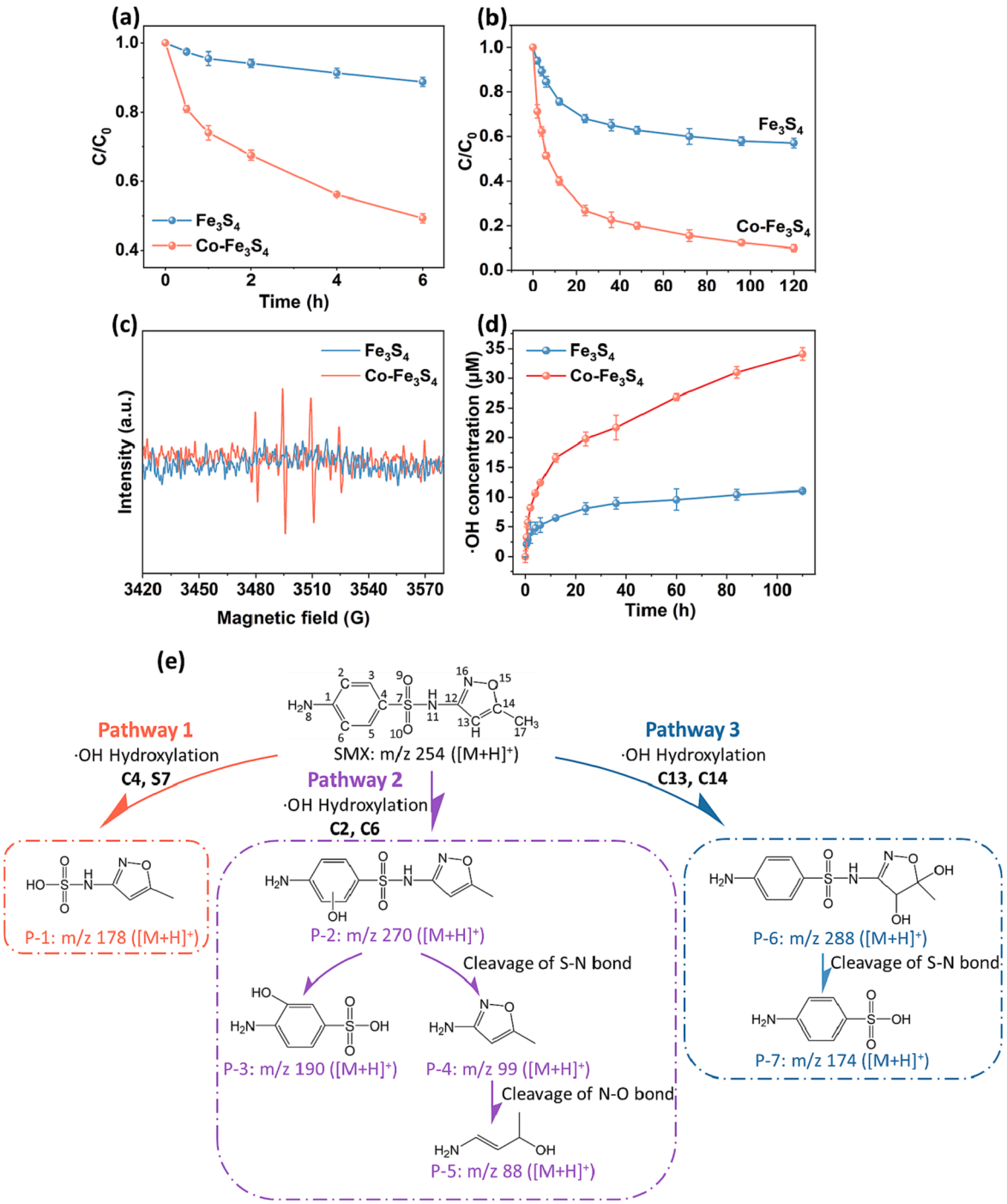

Fig. 2. The (a) short-term and (b) long-term degradation efficiency of SMX by Fe_3S_4 and Co-Fe_3S_4. (reaction condition: [catalyst] = 0.5 g/L, $[SMX]_0$ = 10 mg/L, initial pH = 5.0 ± 0.1) (c) EPR spectra of DMPO-·OH in Fe_3S_4 and Co-Fe_3S_4 systems ($[DMPO]_0$ = 160 mM). (d) Long-term BA probe experiment in Fe_3S_4 and Co-Fe_3S_4 systems. (e) The degradation pathways of SMX in Co-Fe_3S_4.

electrons transferring between O_2 and Co-Fe_3S_4 to hamper the generation of ROS, leading to the drop of SMX degradation efficiency. As shown in Fig. 2a, Co-Fe_3S_4 (with 20% Co) exhibited an outstanding SMX degradation efficiency with a first-order rate constant of $1.92 \times 10^{-3} h^{-1}$, which was a 7.33-fold improvement compared to Fe_3S_4 ($2.6 \times 10^{-4} h^{-1}$). Particularly, over 90% of SMX could be removed by Co-Fe_3S_4 in the long-run experiment, while only 43.6% of SMX was degraded by Fe_3S_4 (Fig. 2b). Co-Fe_3S_4 demonstrates excellent remediation capability without adding additional oxidants (e.g., H_2O_2).

To further reveal the underlying mechanisms of Co-Fe_3S_4 catalyzed degradation, the intermediate degradation products of SMX were identified by UHPLC-QTOF-MS. As shown in Fig. 2e, SMX was degraded mainly through hydroxylation reactions. In Pathway 1, P-1 was produced by breaking the C4-S7 bond, which exhibited relatively weak bond energy and was highly vulnerable to electrophilic species[49] (e.g., •OH). While P-2 was formed by the electrophilic replacement on C2 or C6 of the aromatic ring (Pathway 2), which was one of the classical •OH-mediated degradation pathways of SMX[31,50]. Similar to Pathway 2, dihydroxylated P-6 in Pathway 3 could be generated by hydroxylation reaction on the isoxazole ring[51]. P-2 with hydroxy replacement was the dominant pathway and demonstrated a •OH-triggered SMX degradation.

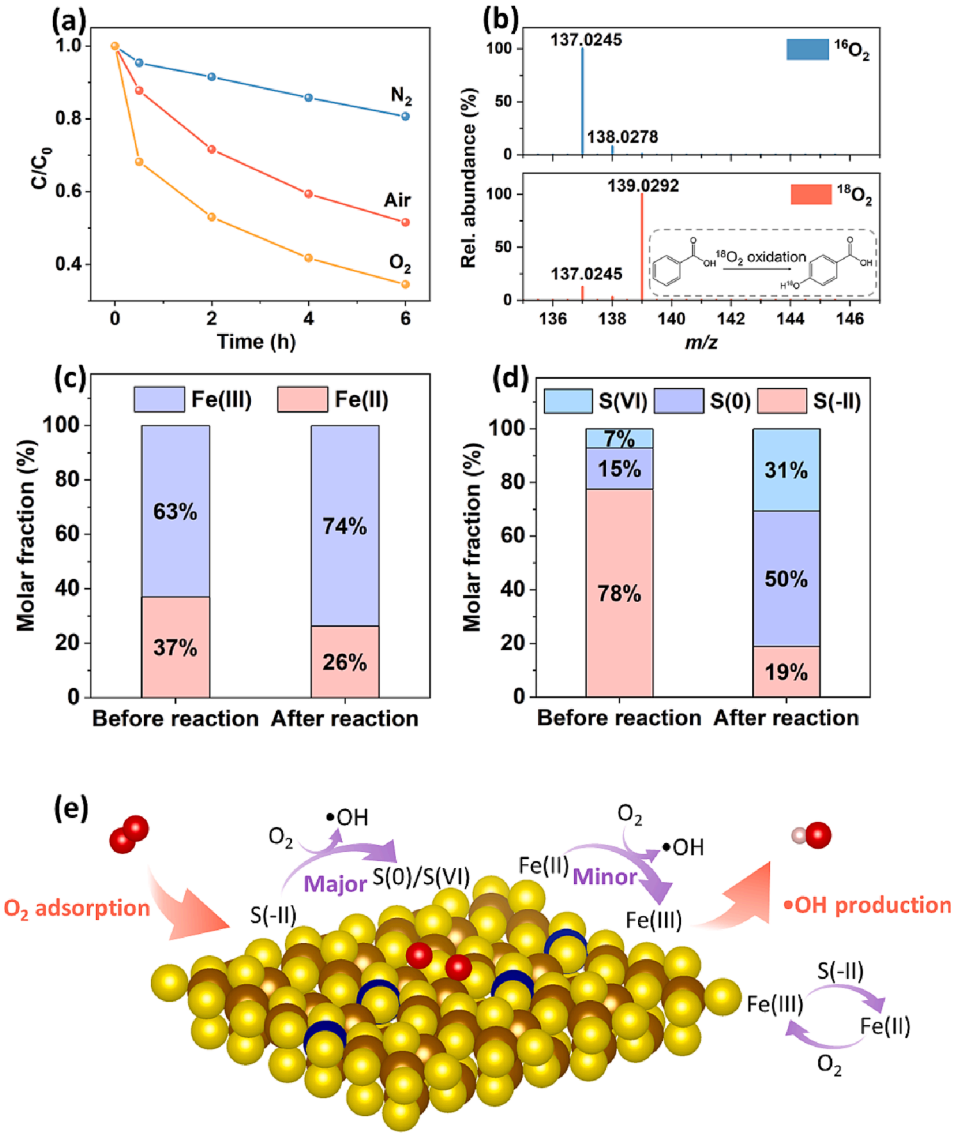

Fig. 3. (a) SMX degradation under different atmospheric conditions (reaction condition: [catalyst] = 0.5 g/L, $[SMX]_0$ = 10 mg/L, initial pH = 5.0 ± 0.1) (b) Mass spectra of HBA under $^{16}O_2$ and $^{18}O_2$ isotope atmosphere conditions. The molar fraction of (c) Fe and (d) S speciation in Co-Fe_3S_4 before and after reaction determined by XPS. (e) Proposed mechanism for O_2 activation in Co-Fe_3S_4 system.

To confirm the contribution of •OH in the degradation of SMX by Co-Fe_3S_4, DMPO was applied as the spin-trapping agent to *in situ* capture •OH. Evident quartet peaks with an intensity ratio of 1:2:2:1 were detected in EPR spectra (Fig. 2c), demonstrating the formation of •OH induced by Co-Fe_3S_4. As a control, no obvious signals of DMPO-•OH adduct were observed in Fe_3S_4's EPR spectra. The contribution of $\bullet O_2^-$ and $^1O_2$ were also investigated via EPR measurements (Fig.S9), however, no relevant signals were found, suggesting the dominant role played by •OH in the degradation of SMX by Co-Fe_3S_4. Quenching experiments by 1 mM and 10 mM of TBA was further applied to verify the contribution of •OH (Fig.S10). Obvious inhabitation of SMX degradation under TBA presence could strongly prove the SMX degradation induced by •OH. In addition, a BA probe reaction was carried out to further quantitatively assess the yield of •OH (Fig. 2d). •OH was rapidly formed in the first 12 h with catalyzation of Co-Fe_3S_4, and the yield (16.63 μM) was enhanced by 3 fold compared to the Fe_3S_4 system (6.05 μM). Furthermore, Co-Fe_3S_4 continuously induced the generation of •OH in the long-run experiment with a total yield of 34.12 μM within 5 days, while only negligible •OH were produced in Fe_3S_4 system in the long-run period. Therefore, Co-Fe_3S_4 could boost the •OH production for the long-lasting remediation of antibiotics without additional oxidants.

3.3. Directional electron transfer between S(-II) and oxygen molecules

To reveal the mechanisms of •OH formation, the degradation experiments were conducted under different atmospheres (Fig. 3a) with dissolved oxygen concentration varied from 4.08 mg/L, 8.84 mg/L to 10.25 mg/L under N_2, air and O_2 atmosphere, respectively. The first-order rate constant of SMX degradation increased from 1.92 × $10^{-3}h^{-1}$ to 2.64 × $10^{-3}h^{-1}$ when the solution was exposed to a pure O_2 atmosphere, and decreased severely to 5.62 × $10^{-4}h^{-1}$ under an N_2 atmosphere. In addition, BA probe experiment was carried out to quantitatively assess the •OH production under different atmospheres (Fig.S11). The yield of •OH was boosted obviously from 9.21 μM to 23.64 μM in the first 6 h under O_2 atmosphere and was severely inhibited under N_2 atmosphere (1.92 μM), consistent with SMX degradation performance. Obviously, O_2 played a critical role in the •OH-mediated degradation of SMX. To further identify the origin of •OH, ^{18}O isotopic labeling study was conducted by analyzing the molecular mass of •OH's probe (BA + •OH → 4-HBA) under $^{16}O_2$ and $^{18}O_2$ atmosphere

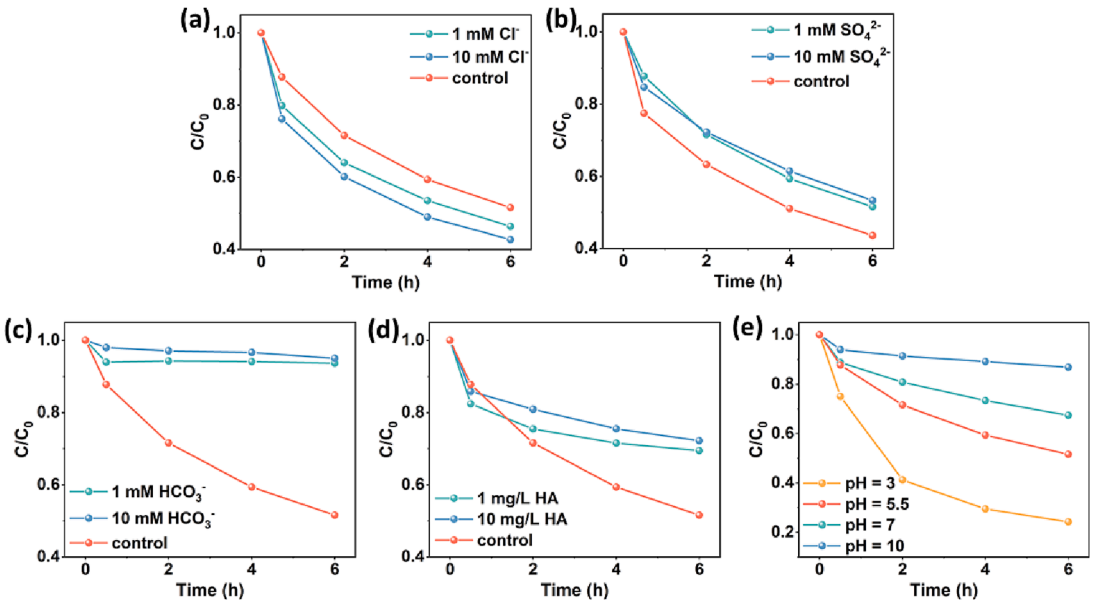

Fig. 4. Effect of coexisting substances (a) Cl^-, (b) SO_4^{2-}, (c) HCO_3^-, and (d) HA and (e) pH on SMX degradation by Co-Fe_3S_4 system (reaction condition: [catalyst] = 0.5 g/L, $[SMX]_0$ = 10 mg/L, initial pH = 5.0 ± 0.1).

(Fig. 3b). Under $^{16}O_2$ atmospheric condition, only 4-$HBA_{m/z=137}$ was detected with an abundance of 92.7%. However, ^{18}O-labeled 4-$HBA_{m/z=139}$ (88% abundance) was the dominant 4-HBA detected under $^{18}O_2$ atmosphere, while 4-$HBA_{m/z=137}$ was the minor species accounting for 11.1%. According to the secondary mass spectrometry (Fig.S12), ^{18}O atom was anchored on the para hydroxy in 4-HBA, which further confirming the generation of ^{18}O-labeled •OH. Hence, the dominant presence of ^{18}O-labeled 4-HBA under $^{18}O_2$ atmosphere strongly demonstrated the origin of •OH was derived from O_2 molecules. Together with the DFT theoretical calculation, Co-Fe_3S_4 favors O_2 dissociative adsorption and further facilitates the electron transferring to the surface-bound O• (Eq.1). Hydrogen atoms ionized from Fe_3S_4 (Eq.2) combined directly with surface-bound O• to form •OH radicals (Eq.3). [52].

$$O_2 \rightarrow 2\ \text{Co-}Fe_3S_4\text{-O}\bullet \quad (1)$$

$$Fe_3S_4 + O_2 + H_2O \rightarrow Fe^{2+} + SO_4^{2-} + H^+ \quad (2)$$

$$\text{Co-}Fe_3S_4\text{-O}\bullet + e^- + H^+ \rightarrow \text{Co-}Fe_3S_4\text{-OH}\bullet \quad (3)$$

Meanwhile, we further investigated the electron donor in the O_2 activation considering the redox potential and electron transfer capacity. The structural Fe(II) of iron-sulfur minerals was widely considered as the electron donor[27,35,52] ($E_{Fe(III)/Fe(II)}$ = 0.77 V), while rare attention has been directed to the structural S(-II), which also poses strong capability to donate an electron ($E_{S(0)/S(-II)}$ = -0.47 V, $E_{S(VI)/S(-II)}$ = -0.68 V)[53]. By itself, Co(II) with a higher redox potential ($E_{Co(III)/Co(II)}$ = 1.92 V) is thermodynamically unfavorable for O_2 activation. Thus, the molar proportion of structural Fe and S species before and after the reaction (Fig. 3c and 3d) was determined by XPS (Fig.S13). During the 6-hour reaction, 11% of structural Fe(II) in Co-Fe_3S_4 was converted to Fe (III) to provide 1.19 μM electrons, which was far from the total electron demand for •OH generation (12.42 μM). Notably, the S species distribution was changed dramatically (Fig. 3d), showing a significant conversion of S(-II) into S(0) and S(VI). The formation of S(0) was monitored along the reaction (Fig.S14), which aligned with the generation of •OH. 35% of structural S(-II) in Co-Fe_3S_4 was converted to 3.75 μM S(0) to supply 7.50 μM electrons, while another 24% S(-II) was oxidized to S(VI) to donate another 20.57 μM electrons. Therefore, structural S(-II) in Co-Fe_3S_4 donated together 28.07 μM electrons, which could not only meet the demand of directionally transfer electrons to O_2 for •OH generation, but also contribute to the Fe(III)/Fe(II) cycling.

Overall, the O_2 activation by Co-Fe_3S_4 was illustrated in Fig. 3e. According to the DFT calculation, O_2 could spontaneously be adsorbed and dissociated on the surface Fe(II) and S(-II) sites of Co-Fe_3S_4. Then, through directional electron transfer and protonation, •OH could be produced through surface-bound •O. Contrary to previous research that O_2 activation was led by Fe(II) oxidation, structural S(-II) proved to play a vital role in donating electrons not only directionally to O_2 activation, but also to Fe(III) reduction. The majority of directional electron transfer was drawn from structural S(-II) instead of Fe(II).

3.4. Remediation performance under different environmental conditions

As shown in Fig. 4, the presence of SO_4^{2-} and Cl^- exhibited a small effect on the degradation of SMX, with 10 mM Cl^- enhancing degradation by 8.8 % and 10 mM SO_4^{2-} inhibiting it by 7.9 %. However, the presence of 10 mM HCO_3^- or even 1 mg/L HA induced inhibitory effects on the remediation performance of Co-Fe_3S_4. Owing to the relatively high rate constant ($k_{HCO_3^-}$ = 1.5 × $10^7 LM^{-1}s^{-1}$)[54], HCO_3^- would compete for •OH, which would result in faster consumption of •OH and a 43.4% of reduction in the degradation efficiency of SMX by 10 mM HCO_3^-. The presence of HA likely covered the Co-Fe_3S_4 surface, preventing adsorption of O_2[55], which significantly reduced •OH generation and the removal of SMX (decreased from 48.4% to 27.8%). Additionally, Co-Fe_3S_4 posed robust remediation performance across a wide pH range (pH = 3–7), but was less effective under very alkaline conditions. 75.8% SMX could be effectively degraded with an initial pH of 3.0 (Fig. 4e). While, the formation and precipitation of ferric hydroxide under the alkaline conditions would occupy Co-Fe_3S_4's active sites, inhibiting the adsorption and activation of O_2.

In addition, Co-Fe_3S_4/O_2 system possessed an efficient remediation performance to low-concentration antibiotics. The degradation efficiency of 200 ppb SMX reached 67.7% within 6 h, and the total removal of mixed low-concentration antibiotics (including 200 ppb of SMX, SDZ, CBZ and OFX) was up to 99.7% (Fig.S15). The remediation performance in actual water bodies was also evaluated using secondary effluent collected from a wastewater treatment plant in Shenzhen, China. Co-Fe_3S_4/O_2 system maintained a high removal (up to 99.6%) on low-concentration antibiotics in secondary effluent (Fig. S15), demonstrating the potential practical application of Co-Fe_3S_4/O_2 system for

environmental remediation.

The reusability of the Co-Fe_3S_4/O_2 system was also investigated, and Co-Fe_3S_4 could maintain stable performance on the degradation of SMX in the first two cycles (Fig. S16a). The degradation efficiency's gradual decrease could be attributed to the loss of Co-Fe_3S_4's reactive sites, as slight passivation was observed in the used Co-Fe_3S_4's surface (Fig. S16c) with mild changes in crystallization (Fig. S16b).

4. Conclusions

In summary, Co-Fe_3S_4 was successfully synthesized and characterized, and the superior SMX degradation performance of Co-Fe_3S_4 over Fe_3S_4 through the activation of dissolved oxygen molecules has been thoroughly investigated. Guided by DFT calculation that Co doping in Fe_3S_4 could significantly accelerate the adsorption and activation of O_2 on the surface of Fe_3S_4, Co-Fe_3S_4 was synthesized. The novel material resulted in a 7.33-fold of improvement in the SMX degradation, due to both the superior O_2 adsorption and generation of •OH. ROS-induced oxidation of SMX was verified according to the analysis of degradation intermediates, and then •OH was proven to be the dominant ROS and could be continuously generated by the Co-Fe_3S_4 system. Degradation experiments under different atmospheres (i.e., air, O_2, N_2) and $^{18}O_2$ isotopic experiments were further carried out to demonstrate that dissolved oxygen molecules are the source of •OH. In addition to the structural Fe(II), S(-II) in the Co-Fe_3S_4 also contributed to the directional electron transfer to the oxygen molecules. In addition, another essential role of S(-II) was to reduce Fe(III) and promote the iron cycle.

Without the external addition of oxidants (such as H_2O_2 and O_3), Co-Fe_3S_4 can generate in-situ •OH through activation of dissolved oxygen molecules. The performance and mechanism of oxygen activation by Co-Fe_3S_4 and the important role S(-II) played were thoroughly investigated. This work provided new insights into the contribution of oxygen molecules activation in antibiotics remediation and the application of in-situ generated •OH by iron-sulfide materials in water quality control.

Declaration of Competing Interest

The authors declare that they have no known competing financial interests or personal relationships that could have appeared to influence the work reported in this paper.

Data availability

Data will be made available on request.

Acknowledgements

This research was financially supported by the National Natural Science Foundation of China (42077293 and 22006088), Shenzhen Municipal Science and Technology Innovation Committee (JCYJ20190809181413713 and RCYX20210609104448111), Natural Science Foundation of Guangdong Province (2019QN01L797), and Tsinghua Shenzhen International Graduate School (HW2020002 and QD2021010N).

Appendix A. Supplementary data

Details regarding material characterization (Text. S1); analytical methods (Text. S2); Differential charge density of O_2 adsorption on the surface of Co-Fe_3S_4 (Fig. S1); SEM of Fe_3S_4 and Co-Fe_3S_4 (Fig. S2); SEM-EDS of Co-Fe_3S_4 (Fig. S3); XRD of Fe_3S_4 and Co-Fe_3S_4 (Fig. S4); TEM of Co-Fe_3S_4 (Fig. S5); Remediation performance of Co-Fe_3S_4 to different antibiotics, including sulfamethoxazole (SMX), sulfadiazine (SDZ), carbamazepine (CBZ), and ofloxacin (OFX) (Fig. S6); SMX degradation efficiency of Co-Fe_3S_4 with different Cobalt proportions (Fig. S7); XRD and SEM of Co-Fe_3S_4 with different cobalt proportions (Fig. S8); EPR spectra of TEMP-$^1O_2$ and DMPO-•O_2^- (Fig. S9); Quenching experiments of •OH (Fig. S10); BA probe experiment in Co-Fe_3S_4 system under air, N_2 and O_2 atmosphere (Fig. S11); Secondary mass spectra of HBA under $^{16}O_2$ and $^{18}O_2$ conditions (Fig. S12); XPS spectra of Co-Fe_3S_4 before and after reaction (Fig. S13); S_0 concentration in Fe_3S_4 and Co-Fe_3S_4/O_2 systems (Fig. S14); Degradation efficiency of low-concentrated antibiotics (Fig. S15); Reusability of Co-Fe_3S_4 (Fig. S16); Element proportion of Co-Fe_3S_4 according to SEM-EDS (Table. S1). Supplementary data to this article can be found online at https://doi.org/10.1016/j.cej.2023.142465.

References

[1] C. Fu, B. Xu, H. Chen, X. Zhao, G. Li, Y. Zheng, W. Qiu, C. Zheng, L. Duan, W. Wang, Occurrence and Distribution of Antibiotics in Groundwater, Surface Water, and Sediment in Xiong'an New Area, China, and Their Relationship with Antibiotic Resistance Genes, Sci. Total Environ. 807 (2022), 151011, https://doi.org/10.1016/j.scitotenv.2021.151011.

[2] K. Kümmerer, Antibiotics in the Aquatic Environment – A Review – Part I, Chemosphere 75 (4) (2009) 417–434, https://doi.org/10.1016/j.chemosphere.2008.11.086.

[3] J. Xu, Y. Zhang, C. Zhou, C. Guo, D. Wang, P. Du, Y. Luo, J. Wan, W. Meng, Distribution, Sources and Composition of Antibiotics in Sediment, Overlying Water and Pore Water from Taihu Lake, China, Sci. Total Environ. 497–498 (2014) 267–273, https://doi.org/10.1016/j.scitotenv.2014.07.114.

[4] S.-C. Kim, K. Carlson, Temporal and Spatial Trends in the Occurrence of Human and Veterinary Antibiotics in Aqueous and River Sediment Matrices, Environ. Sci. Technol. 41 (1) (2007) 50–57, https://doi.org/10.1021/es060737+.

[5] B.M. Sharma, J. Bečanová, M. Scheringer, A. Sharma, G.K. Bharat, P.G. Whitehead, J. Klánová, L. Nizzetto, Health and Ecological Risk Assessment of Emerging Contaminants (Pharmaceuticals, Personal Care Products, and Artificial Sweeteners) in Surface and Groundwater (Drinking Water) in the Ganges River Basin, India, Sci. Total Environ. 646 (2019) 1459–1467, https://doi.org/10.1016/j.scitotenv.2018.07.235.

[6] Z. Wang, M. Han, E. Li, X. Liu, H. Wei, C. Yang, S. Lu, K. Ning, Distribution of Antibiotic Resistance Genes in an Agriculturally Disturbed Lake in China: Their Links with Microbial Communities, Antibiotics, and Water Quality, J. Hazard. Mater. 393 (2020), 122426, https://doi.org/10.1016/j.jhazmat.2020.122426.

[7] S.M. Zainab, M. Junaid, N. Xu, R.N. Malik, Antibiotics and Antibiotic Resistant Genes (ARGs) in Groundwater: A Global Review on Dissemination, Sources, Interactions, Environmental and Human Health Risks, Water Res. 187 (2020), 116455, https://doi.org/10.1016/j.watres.2020.116455.

[8] C. Dai, S. Li, Y. Duan, K.H. Leong, S. Liu, Y. Zhang, L. Zhou, Y. Tu, Mechanisms and Product Toxicity of Activated Carbon/Peracetic Acid for Degradation of Sulfamethoxazole: Implications for Groundwater Remediation, Water Res. 216 (2022), 118347, https://doi.org/10.1016/j.watres.2022.118347.

[9] Y. Li, X. Zhao, Y. Yan, J. Yan, Y. Pan, Y. Zhang, B. Lai, Enhanced Sulfamethoxazole Degradation by Peroxymonosulfate Activation with Sulfide-Modified Microscale Zero-Valent Iron (S-MFe0): Performance, Mechanisms, and the Role of Sulfur Species, Chem. Eng. J. 376 (2019), 121302, https://doi.org/10.1016/j.cej.2019.03.178.

[10] W. Guo, Q. Zhao, J. Du, H. Wang, X. Li, N. Ren, Enhanced Removal of Sulfadiazine by Sulfidated ZVI Activated Persulfate Process: Performance, Mechanisms and Degradation Pathways, Chem. Eng. J. 388 (2020), 124303, https://doi.org/10.1016/j.cej.2020.124303.

[11] Z. Jiang, X. Tan, J. Xu, Y. Huang, Piezoelectric-Induced Internal Electric Field in Bi2WO6 Nanoplates for Boosting the Photocatalytic Degradation of Organic Pollutants, ACS Appl. Nano Mater. 5 (5) (2022) 7588–7597, https://doi.org/10.1021/acsanm.2c01698.

[12] S. Akbari, F. Ghanbari, M. Moradi, Bisphenol A Degradation in Aqueous Solutions by Electrogenerated Ferrous Ion Activated Ozone, Hydrogen Peroxide and Persulfate: Applying Low Current Density for Oxidation Mechanism, Chem. Eng. J. 294 (2016) 298–307, https://doi.org/10.1016/j.cej.2016.02.106.

[13] G.P. Anipsitakis, D.D. Dionysiou, Degradation of Organic Contaminants in Water with Sulfate Radicals Generated by the Conjunction of Peroxymonosulfate with Cobalt, Environ. Sci. Technol. 37 (20) (2003) 4790–4797, https://doi.org/10.1021/es0263792.

[14] A.P. Bhat, P.R. Gogate, Degradation of Nitrogen-Containing Hazardous Compounds Using Advanced Oxidation Processes: A Review on Aliphatic and Aromatic Amines, Dyes, and Pesticides, J. Hazard. Mater. 403 (2021), 123657, https://doi.org/10.1016/j.jhazmat.2020.123657.

[15] H. Fu, P. Tan, R. Wang, S. Li, H. Liu, Y. Yang, Z. Wu, Advances in Organophosphorus Pesticides Pollution: Current Status and Challenges in Ecotoxicological, Sustainable Agriculture, and Degradation Strategies, J. Hazard. Mater. 424 (2022), 127494, https://doi.org/10.1016/j.jhazmat.2021.127494.

[16] X. Wang, J. Jing, M. Zhou, R. Dewil, Recent Advances in H2O2-Based Advanced Oxidation Processes for Removal of Antibiotics from Wastewater, Chin. Chem. Lett. 34 (3) (2023) 107621.

[17] X. Tan, W. Ding, Z. Jiang, L. Sun, Y. Huang, Reinventing MoS2 Co-Catalytic Fenton Reaction: Oxygen-Incorporation Mediating Surface Superoxide Radical Generation, Nano Res. 15 (3) (2022) 1973–1982, https://doi.org/10.1007/s12274-021-3848-3.

[18] L. Sun, X. Tan, W. Ding, Y. Huang, Emerging Investigator Series: Hetero-Phase Junction 1T/2H-MoS $_2$ Nanosheets Decorated by FeOOH Nanoparticles for Enhanced Visible Light Photo-Fenton Degradation of Antibiotics, Environ. Sci. Nano 9 (7) (2022) 2342–2350, https://doi.org/10.1039/D2EN00045H.
[19] R. Pelalak, R. Alizadeh, E. Ghareshabani, Z. Heidari, Degradation of Sulfonamide Antibiotics Using Ozone-Based Advanced Oxidation Process: Experimental, Modeling, Transformation Mechanism and DFT Study, Sci. Total Environ. 734 (2020), 139446, https://doi.org/10.1016/j.scitotenv.2020.139446.
[20] C.V. Rekhate, J.K. Srivastava, Recent Advances in Ozone-Based Advanced Oxidation Processes for Treatment of Wastewater- A Review, Chem. Eng. J. Adv. 3 (2020), 100031, https://doi.org/10.1016/j.ceja.2020.100031.
[21] J. Lee, U. von Gunten, J.-H. Kim, Persulfate-Based Advanced Oxidation: Critical Assessment of Opportunities and Roadblocks, Environ. Sci. Technol. 54 (6) (2020) 3064–3081, https://doi.org/10.1021/acs.est.9b07082.
[22] Z. Zhou, X. Liu, K. Sun, C. Lin, J. Ma, M. He, W. Ouyang, Persulfate-Based Advanced Oxidation Processes (AOPs) for Organic-Contaminated Soil Remediation: A Review, Chem. Eng. J. 372 (2019) 836–851, https://doi.org/10.1016/j.cej.2019.04.213.
[23] G. Chen, H. Wang, W. Dong, W. Ding, F. Wang, Z. Zhao, Y. Huang, The Overlooked Role of Co(OH)2 in Co3O4 Activated PMS System: Suppression of Co2+ Leaching and Enhanced Degradation Performance of Antibiotics with RGO, Sep. Purif. Technol. 304 (2023), 122203, https://doi.org/10.1016/j.seppur.2022.122203.
[24] A. Serrà, L. Philippe, F. Perreault, S. Garcia-Segura, Photocatalytic Treatment of Natural Waters. Reality or Hype? The Case of Cyanotoxins Remediation, Water Res. 188 (2021), 116543, https://doi.org/10.1016/j.watres.2020.116543.
[25] M. Diana, M. Felipe-Sotelo, T. Bond, Disinfection Byproducts Potentially Responsible for the Association between Chlorinated Drinking Water and Bladder Cancer: A Review, Water Res. 162 (2019) 492–504, https://doi.org/10.1016/j.watres.2019.07.014.
[26] A.F. Gilca, C. Teodosiu, S. Fiore, C.P. Musteret, Emerging Disinfection Byproducts: A Review on Their Occurrence and Control in Drinking Water Treatment Processes, Chemosphere 259 (2020), 127476, https://doi.org/10.1016/j.chemosphere.2020.127476.
[27] D. Cheng, A. Neumann, S. Yuan, W. Liao, A. Qian, Oxidative Degradation of Organic Contaminants by FeS in the Presence of O $_2$, Environ. Sci. Technol. 54 (7) (2020) 4091–4101, https://doi.org/10.1021/acs.est.9b07012.
[28] L. Wu, Z. Sun, Y. Zhen, S. Zhu, C. Yang, J. Lu, Y. Tian, D. Zhong, J. Ma, Oxygen Vacancy-Induced Nonradical Degradation of Organics: Critical Trigger of Oxygen (O2) in the Fe–Co LDH/Peroxymonosulfate System, Environ. Sci. Technol. 55 (22) (2021) 15400–15411, https://doi.org/10.1021/acs.est.1c04600.
[29] D. Cheng, S. Yuan, P. Liao, P. Zhang, Oxidizing Impact Induced by Mackinawite (FeS) Nanoparticles at Oxic Conditions Due to Production of Hydroxyl Radicals, Environ. Sci. Technol. 50 (21) (2016) 11646–11653, https://doi.org/10.1021/acs.est.6b02833.
[30] R. Long, K. Mao, X. Ye, W. Yan, Y. Huang, J. Wang, Y. Fu, X. Wang, X. Wu, Y. Xie, Y. Xiong, Surface Facet of Palladium Nanocrystals: A Key Parameter to the Activation of Molecular Oxygen for Organic Catalysis and Cancer Treatment, J. Am. Chem. Soc. 135 (8) (2013) 3200–3207, https://doi.org/10.1021/ja311739v.
[31] J. Liu, C. Xiong, S. Jiang, X. Wu, S. Song, Efficient Evolution of Reactive Oxygen Species over the Coordinated π-Delocalization g-C3N4 with Favorable Charge Transfer for Sustainable Pollutant Elimination, Appl. Catal. B Environ. 249 (2019) 282–291, https://doi.org/10.1016/j.apcatb.2019.03.014.
[32] R. Zhu, J. Ding, Y. Xu, J. Yang, Q. Xu, H. Pang, π-Conjugated Molecule Boosts Metal-Organic Frameworks as Efficient Oxygen Evolution Reaction Catalysts, Small 14 (50) (2018) 1803576, https://doi.org/10.1002/smll.201803576.
[33] M. Ali, M. Danish, M. Tariq, A. Ahmad, K. Shahzad Ayub, S. Lyu, Mechanistic Insights into the Degradation of Trichloroethylene by Controlled Release Nano Calcium Peroxide Activated by Iron Species Coupled with Nano Iron Sulfide, Chem. Eng. J. 399 (2020), 125754, https://doi.org/10.1016/j.cej.2020.125754.
[34] W. Liu, J. Tian, C. Mao, Z. Wang, J. Liu, R.A. Dahlgren, L. Zhang, X. Wang, Sulfur Vacancy Promoted Peroxidase-like Activity of Magnetic Greigite (Fe3S4) for Colorimetric Detection of Serum Glucose, Anal. Chim. Acta 1127 (2020) 246–255, https://doi.org/10.1016/j.aca.2020.06.056.
[35] W. Liu, J. Liu, P. Zhou, R.A. Dahlgren, X. Wang, Mechanisms for Hydroxyl Radical Production and Arsenic Removal in Sulfur-Vacancy Greigite (Fe3S4), J. Colloid Interface Sci. 606 (2022) 688–695, https://doi.org/10.1016/j.jcis.2021.08.072.
[36] Y. Shi, X. Wang, X. Liu, C. Ling, W. Shen, L. Zhang, Visible Light Promoted Fe3S4 Fenton Oxidation of Atrazine, Appl. Catal. B Environ. 277 (2020), 119229, https://doi.org/10.1016/j.apcatb.2020.119229.
[37] S. Wang, J. Zhu, T. Li, F. Ge, Z. Zhang, R. Zhu, H. Xie, Y. Xu, Oxygen Vacancy-Mediated CuCoFe/Tartrate-LDH Catalyst Directly Activates Oxygen to Produce Superoxide Radicals: Transformation of Active Species and Implication for Nitrobenzene Degradation, Environ. Sci. Technol. 56 (12) (2022) 7924–7934, https://doi.org/10.1021/acs.est.2c00522.
[38] M.M. Montemore, M.A. van Spronsen, R.J. Madix, C.M. Friend, O2 Activation by Metal Surfaces: Implications for Bonding and Reactivity on Heterogeneous Catalysts, Chem. Rev. 118 (5) (2018) 2816–2862, https://doi.org/10.1021/acs.chemrev.7b00217.
[39] W. Xiang, M. Huang, Y. Wang, X. Wu, F. Zhang, D. Li, T. Zhou, New Insight in the O2 Activation by Nano Fe/Cu Bimetals: The Synergistic Role of Cu(0) and Fe(II), Chin. Chem. Lett. 31 (10) (2020) 2831–2834, https://doi.org/10.1016/j.cclet.2020.08.006.
[40] Q. Liu, H. Li, H. Zhang, Z. Shen, H. Ji, The Role of Cs Dopants for Improved Activation of Molecular Oxygen and Degradation of Tetracycline over Carbon Nitride, Chin. Chem. Lett. 33 (11) (2022) 4756–4760, https://doi.org/10.1016/j.cclet.2021.12.089.
[41] T. Yan, Q. Yang, R. Feng, X. Ren, Y. Zhao, M. Sun, L. Yan, Q. Wei, Highly Effective Visible-Photocatalytic Hydrogen Evolution and Simultaneous Organic Pollutant Degradation over an Urchin-like Oxygen-Doped $MoS_2/ZnIn_2S_4$ Composite, Front. Environ. Sci. Eng. 16 (10) (2022) 131, https://doi.org/10.1007/s11783-022-1566-z.
[42] Y. Wang, P. Ning, R. Zhao, K. Li, C. Wang, X. Sun, X. Song, Q. Lin, A Cu-Modified Active Carbon Fiber Significantly Promoted H_2S and PH_3 Simultaneous Removal at a Low Reaction Temperature, Front. Environ. Sci. Eng. 15 (6) (2021) 132, https://doi.org/10.1007/s11783-021-1425-3.
[43] H. Li, S. Sun, H. Ji, W. Liu, Z. Shen, Enhanced Activation of Molecular Oxygen and Degradation of Tetracycline over Cu-S4 Atomic Clusters, Appl. Catal. B Environ. 272 (2020), 118966, https://doi.org/10.1016/j.apcatb.2020.118966.
[44] B. Zhao, L.L. Liu, G.D. Cheng, T. Li, N. Qi, Z.Q. Chen, Z. Tang, Interaction of O2 with Monolayer MoS2: Effect of Doping and Hydrogenation, Mater. Des. 113 (2017) 1–8, https://doi.org/10.1016/j.matdes.2016.10.005.
[45] Z.J. Zhang, X.Y. Chen, Magnetic Greigite (Fe3S4) Nanomaterials: Shape-Controlled Solvothermal Synthesis and Their Calcination Conversion into Hematite (α-Fe2O3) Nanomaterials, J. Alloys Compd. 488 (1) (2009) 339–345, https://doi.org/10.1016/j.jallcom.2009.08.127.
[46] N.Y. Dzade, A. Roldan, N.H. de Leeuw, DFT-D2 Study of the Adsorption and Dissociation of Water on Clean and Oxygen-Covered 001 and 011 Surfaces of Mackinawite (FeS), J. Phys. Chem. C 120 (38) (2016) 21441–21450, https://doi.org/10.1021/acs.jpcc.6b06122.
[47] Z. Lu, S. Meng, Y. Pang, G. Xu, D. Ma, S.H. Talib, Z. Yang, Tuning the Activation of O2 on Pt Single-Atom Catalyst Using External-Electric Field: A First-Principles Study, Phys. B Condens. Matter 638 (2022), 413934, https://doi.org/10.1016/j.physb.2022.413934.
[48] Z. Han, S. Zhao, J. Xiao, X. Zhong, J. Sheng, W. Lv, Q. Zhang, G. Zhou, H.-M. Cheng, Engineering D-p Orbital Hybridization in Single-Atom Metal-Embedded Three-Dimensional Electrodes for Li–S Batteries, Adv. Mater. 33 (44) (2021) 2105947, https://doi.org/10.1002/adma.202105947.
[49] T. Luo, J. Wan, Y. Ma, Y. Wang, Y. Wan, Sulfamethoxazole Degradation by an Fe (Ii)-Activated Persulfate Process: Insight into the Reactive Sites, Product Identification and Degradation Pathways, Environ. Sci. Process. Impacts 21 (9) (2019) 1560–1569, https://doi.org/10.1039/C9EM00254E.
[50] X. Long, Z. Xiong, R. Huang, Y. Yu, P. Zhou, H. Zhang, G. Yao, B. Lai, Sustainable Fe(III)/Fe(II) Cycles Triggered by Co-Catalyst of Weak Electrical Current in Fe(III)/Peroxymonosulfate System: Collaboration of Radical and Non-Radical Mechanisms, Appl. Catal. B Environ. 317 (2022), 121716, https://doi.org/10.1016/j.apcatb.2022.121716.
[51] P. Gao, X. Tian, W. Fu, Y. Wang, Y. Nie, C. Yang, Y. Deng, Copper in LaMnO3 to Promote Peroxymonosulfate Activation by Regulating the Reactive Oxygen Species in Sulfamethoxazole Degradation, J. Hazard. Mater. 411 (2021), 125163, https://doi.org/10.1016/j.jhazmat.2021.125163.
[52] X. Li, J. He, J. Lu, Y. Zhou, Y. Zhou, In-Situ Production and Activation of H2O2 for Enhanced Degradation of Roxarsone by FeS2 Decorated Resorcinol-Formaldehyde Resins, J. Hazard. Mater. 424 (2022), 127650, https://doi.org/10.1016/j.jhazmat.2021.127650.
[53] C. Wang, C. Ying, Y. Tang, Y. Yan, X. Feng, Synergistic Effect of Co(II) Doping on FeS Activating Heterogeneous Fenton Processes toward Degradation of Rhodamine B, Chem. Eng. J. Adv. 4 (2020), 100044, https://doi.org/10.1016/j.ceja.2020.100044.
[54] H. Dong, J. Chen, L. Feng, W. Zhang, X. Guan, T.J. Strathmann, Degradation of Organic Contaminants through Activating Bisulfite by Cerium(IV): A Sulfate Radical-Predominant Oxidation Process, Chem. Eng. J. 357 (2019) 328–336, https://doi.org/10.1016/j.cej.2018.09.024.
[55] X.Z. Li, C.M. Fan, Y.P. Sun, Enhancement of Photocatalytic Oxidation of Humic Acid in TiO2 Suspensions by Increasing Cation Strength, Chemosphere 48 (4) (2002) 453–460, https://doi.org/10.1016/S0045-6535(02)00135-2.